The Spatial and Temporal Patterns of the Surface Solar Irradiation in Northeastern Region of Brazil

Francisco José Lopes de Lima[1,2]*, Fernando Ramos Martins[1], Rodrigo Santos Costa[2], André Rodrigues Gonçalves[2], Ana Paula Paes dos Santos[2], Enio Bueno Pereira[2]

[1] Federal University of São Paulo, Santos-SP (Brazil)

[2] Brazilian Institute for Space Research, São José dos Campos (Brazil)

Abstract

Earlier studies have demonstrated that the Northeastern region (NEB) receives the largest surface solar irradiance of the Brazilian territory due to its location in the tropical area and its climate and environment characteristics. The work aimed at investigating the surface solar irradiation variability and trends and relates it with regional climate and environmental characteristics. The statistical analysis was based on ground data acquired in automated weather stations operated by INMET. A quality control procedure was accomplished according to WMO criteria to avoid suspicious data. The results pointed out a significant variability in seasonal and annual scales. The cluster analysis methodology was performed and provided five regional patterns concerning the incoming solar irradiation. There are quite interesting temporal complementary regimes in the region. From December to February, the surface solar irradiation average achieves simultaneously its maximum in the southeastern area and its minimum in the western area of NEB. The Mann-Kendall method and the Sen technique were used to evaluate the annual and seasonal trends of the surface solar irradiation averages. The surface solar irradiation in the southeastern area of NEB is decreasing by 50 Wh/m²/year since 2008. On the other hand, it is increasing around 40 Wh/m²/year in the semi-arid area along the same timeframe.
.

Keywords: Solar Irradiation, Analysis of Clustering, Seasonal and Interannual.

1. Introduction

The study of the incoming solar radiation has direct implications on the meteorology, especially on the climate variability (Lohmann et al., 2016). The solar radiation is the energy resource for every physical and biological process regulating the life in Earth including the diurnal and seasonal cycles of temperature and the photosynthesis (Lima et al., 2007). The evapotranspiration is intrinsically related to the Earth's energy balance, and the solar energy data allows to quantify the energy allocated to heat soil and atmosphere (Silva et al., 2005). The surface solar radiation also plays an important role in carbon assimilation by canopies and, consequently, in the productivity of the ecosystems (Cohen et al., 2002; Gu, 2003; Roderick et al., 2001; V. de P. R. da Silva et al., 2010; R. A. E. Silva et al., 2010).

In addition, the solar radiation has also an important role in several human activities with important environmental and socioeconomic consequences like agriculture, engineering, architecture, energy generation and consumption and other sectors (Wild, 2009).

Currently, the world's primary energy demand relies largely on fossil fuels. The consumption of fossil fuels releases a large quantity of greenhouse gases into the atmosphere, especially carbon oxides. The Brazilian energy matrix is already an exemplary case of renewable energy usage presenting a large share of hydro, wind and biomass power generation. However, taking into consideration the resumption of economic growth, there will be an increasing energy demand in Brazil (Goldemberg and Lucon, 2008). The renewable energy sources, especially solar and wind power, are an important alternative not only because of the inherent advantages related to energy matrix diversification but also there will be great worldwide pressure to stabilize carbon emissions rate in the atmosphere through reducing the consumption of fossil fuels.

Nowadays, the solar energy is already considered an alternative to complement the Brazilian energy matrix based on mostly hydroelectric and thermoelectric power plants (Pereira et al., 2006). The conversion of solar radiation

into electricity or thermal energy reduces the environmental impacts and emission of pollutants during the operation of the power plants. However, in addition to the unsolved technological difficulties related to the temporal intermittency and dependence on weather conditions, the investments to install and operate solar power plants are still larger than the required for the conventional hydropower and thermal power plants (Pereira et al. 2017).

Thus, the solar energy will not replace the fossil fuels or hydroelectric power in the current scenario, but it will be gradually added to complement the current sources through hybrid and distributed generation systems (Goldemberg and Lucon, 2008). The current limitations on solar energy exploitation tend to be reduced or even eliminated, mainly in response to technological development and to the growth of world energy demand in developing countries.

Brazil is a country located mostly in the intertropical region and, consequently, it has a large solar energy potential throughout its territory. Despite of that, reliable database on surface solar irradiance are still scarce in the country. Several studies faced many limitations due to the low density of radiometric stations in the Brazilian territory (Echer et al., 2006; Lima et al., 2016; Martins et al., 2007; Martins and Pereira, 2011). However, reliable solar energy assessments are an important tool to understand the uncertainties associated with the spatial and temporal variabilities of solar energy resource. In addition to that, the methodologies to provide reliable short-term forecasts of solar energy are gaining great importance to support the energy sector for both planning and operation of the solar generation plants and country's electricity grid system (F. R. Martins et al., 2008; F.R. Martins et al., 2008; Martins and Pereira, 2006).

In this context, the present work provides information and knowledge on the spatial variability of the surface solar irradiation in the Northeastern region of Brazil (NEB). The study aimed at identifying consistent time series of surface solar irradiation data acquired by the National Institute of Meteorology (INMET) using reliable ground data acquired by the automated weather stations operating in NEB territory from 2008 to 2015. It also aimed at investigating the climatological trends presented by surface solar radiation data. The results can provide information for several issues of great relevance: better understanding and knowledge on the solar energy availability and variability; providing the energy sector with reliable solar radiation data and specialized meteorological services to support the solar energy deployment in the Brazilian Northeastern region.

2. Material and Methods

This chapter is segmented in the following topics to facilitate comprehension of the work development: the study area; the data qualification procedure; the cluster analysis; the evaluation of inter-annual variability and trend analysis.

2.1   Study area: Brazilian Northeastern region (NEB)

The Northeastern region of Brazil presents a wide variety of climate and anthropic features affecting the incoming solar irradiation. This topic briefly describes the main issues, but the authors recommend reading Cavalcanti et al. (2009) for more detailed description.

The NEB has an area around of 1.56 million km² corresponding to 18% of the Brazilian territory. According to Kayano and Andreoli (2009), the region is usually described as presenting three major climates (see Figure 1). The humid coastal climate is the typical climate from the coast of Bahia till Rio Grande do Norte. The tropical climate covers the continental area of the states of Bahia, Ceará, Maranhão and Piauí. The semi-arid tropical climate comprises the central area of the region.

The precipitation presents an uneven distribution throughout the year, between 300 and 2000 mm, and great spatial-temporal variability. The precipitation variability is basically associated with regional atmospheric systems such as the Subtropical Anticyclones over the South Atlantic and North Atlantic and the Equatorial Trough (Kayano and Andreoli, 2009). The rainfall regime in the NEB is quite complex presenting three distinct precipitation patterns illustrated at the Figure 1. The rain occurs from February to April in the North of the NEB (States of Ceará, Rio Grande do Norte, interior of Paraíba and Pernambuco) linked to the displacement of the Intertropical Convergence Zone (ITCZ) to the south (Kousky, 1979; Molion and Bernardo, 2002). The precipitation over Eastern coast occurs from May to June (from Rio Grande do Norte to Bahia) and it is related to the influence of the tropical air masses and easterly waves disturbances (EWD). It is also important to mention

that sea breeze also has an important contribution to precipitation rates in the coastal areas. Finally, the precipitation in the continental area (including Bahia, Pernambuco and southern areas of Maranhão, Piauí) occurs from November to December due to the influence of frontal systems, local convection, and cyclonic vortices.
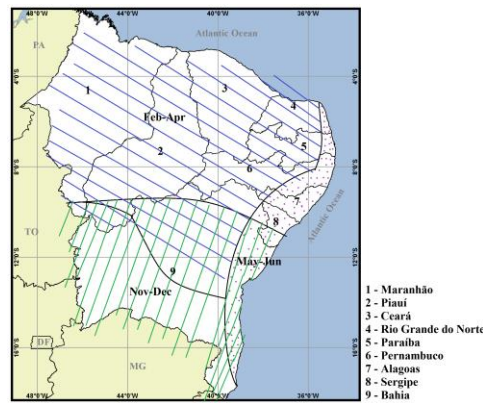
Figure 1. Spatial and temporal distribution of precipitation in NEB territory. The months in which the average monthly precipitation reaches the maximum of rainfall regimes are describe over each area. Source: adapted by (Kousky, 1979)**.**

The air temperature presents high annual averages in the NEB reaching values between 20° and 28°C. The temperature averages between 24° to 26°C in the areas under 200 m high and in the eastern seaboard. However, in high altitude areas (see Figure 2), like Chapada Diamantina and the Borborema Plateau, the annual mean temperature reaches values below 20°C (Kayano and Andreoli, 2009; Pereira et al., 2006). The incidence of solar radiation is large all year round presenting annual average around 5.5 kWh/m².dia for global solar irradiation. The NEB is the area presenting the largest solar energy potential according to the Brazilian Atlas of Solar Energy (F.R. Martins et al., 2008; Pereira et al., 2017).

2.2   Observational Data

The solar radiation data used in this work were acquired from January/2005 to December/2015 in 129 automated weather stations (AWS) operated by the National Institute of Meteorology (INMET). The automatic surface weather station includes a data logger unit to store data acquired by several sensors for the following meteorological parameters (atmospheric pressure, air temperature and relative humidity, precipitation, solar radiation, direction and wind speed, etc.). The data acquisition system operates at one-minute frequency but data is stored with one-hour time step. Figure 2 shows the location of the AWS used for this study.
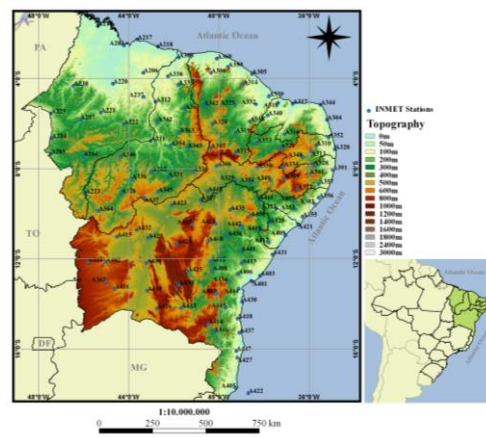
Figure 2. The orography map shows the spatial distribution of the automatic weather stations operated by Brazilian Institute for Meteorology (INMET) in the NEB region.

2.3   Data qualification procedure

Some factors can affect the reliability of the ground observations. Power outage, electrical discharges, environment changes in the site neighborhood and equipment substitution are some of them.

The major quality issue in the AWS's databases was the occurrence of failure acquisition gaps extending for days, months and years. Such gaps are associated with a variety of reasons including low maintenance. All

measurements sites presenting long failure gaps in solar data acquisition were discarded. In addition, a computational script was developed to check if data was physically feasible or extremely rare using threshold criteria established by WMO for BSRN (Baseline Surface Radiation Network) measurement sites (Roesch et al., 2011). We discarded all solar radiation data flagged as suspicious in order to ensure the reliability of solar and meteorological data used in this study.
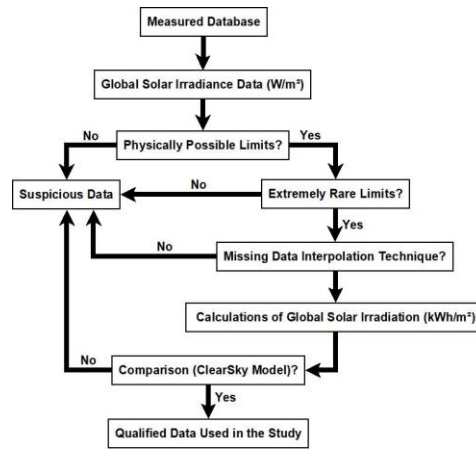
Figure 3. Flowchart of the computational procedure used for quality control of the solar radiation data acquired at the measurement sites in the NEB.

In addition, the authors established a criterion to ensure the database is representative of the typical variability of solar irradiation over the annual cycle. All measuring sites presenting less than 70% of the expected data records for one year-round cycle were discarded. Then the annual, monthly and daily descriptive statistical analyses were performed for the entire timeframe in each of the INMET meteorological stations.

2.4 Interpolation Mapping and Cluster Analysis (CA)

The maps of the surface solar irradiation were prepared using the kriging interpolation of the reliable ground data. Such maps provided information to evaluate the climatology of the incoming solar radiation in NEB and its inherent variability (Dobesch et al., 2010, 2007; Journée and Bertrand, 2010; Mello et al., 2003; Mueller et al., 2004).

The Cluster Analysis (CA) was the statistical approach used to identify homogenous regions based on the similarity of the surface solar irradiation. The CA procedure used a data array containing the monthly average values of the surface solar irradiation and the geographical coordinates assigned to each AWS. The agglomerative hierarchical method based on (Ward, 1963) was used. The hierarchical cluster analysis follows three steps: calculate the Euclidean distances between AWS data arrays, bond the AWS clusters in a dendrogram, and then find the best similarity threshold to establish the homogeneous regions (Corrar et al., 2007; Lima et al., 2010, 2016; Paixao et al., 2011; A. P. P. dos Santos et al., 2016b; Tennant and Hewitson, 2002). Both the number of similar regions and the number of members (AWS) in each of them were obtained subjectively by establishing a threshold in the dendrogram (Hair Jr. et al., 2005).

2.6 Seasonal and Inter-annual Variability and Trend Analysis

The statistical boxplot technique, described by Wilks (2006), was used to evaluate the surface solar irradiation data variability on each homogeneous region. The boxplot provides a complete statistical description: the average and/or median values, the interquartile range and the asymmetry (the difference between quartile and median).

Several studies used the Mann-Kendall method to investigate the climate trends based on historical datasets of meteorological parameters and it is the most appropriate method for climate change studies (dos Santos et al., 2018; Goossens and Beerger, 1986). In summary, the Mann-Kendall method is a non-parametric test to evaluate whether the null hypothesis that each record data is independent and equally distributed, i.e., there is no trend in the dataset. The null hypothesis is rejected if $|Z| > Z_{a/2}$ for significance level equals $\square$. The equations (1) and (2) show the mathematical expression to evaluate Z. In this case, the upward trend occurs for $Z > 0$ and, a downward trend for $Z < 0$.

$$Z = \begin{cases} \dfrac{S-1}{\sqrt{VAR(S)}} & if \quad S > 0 \\ 0 & if \quad S = 0 \\ \dfrac{S+1}{VAR(S)} & if \quad S < 0 \end{cases} \qquad \text{(eq. 1)}$$

where:

$$S = \sum_{k=1}^{n-1} \sum_{j=k+1}^{n} sign(x_j - x_k) \qquad \text{(eq. 2)}$$

where x_j and x_k are two successive data records; j and k ($j > k$) stands for their position in the dataset; and n is the database size. The function *sign* provides three possible outputs: it is 1 (one) if x_j - $x_k > 0$; it is null (0) when the successive data records are equal; and it is (-1) when x_j - $x_{k <} 0$. The *VAR(S)* is obtained from equation (3):

$$VAR(S) = \frac{1}{18}[n(n-1)(2n+5) - \sum_{p=1}^{g}(t_p - 1)(2t_p + 5)] \qquad \text{(eq. 3)}$$

where g is the number of groups with data repetitions and t_p is the number of data in the *p-th* group. (Hisdal et al. 2001; Wu et al. 2008)

We also evaluated the slope and scale of the data trend using the non-parametric method described by Sen according to equation (4) (Sen, 1968; Sneyers, 1990). The method is indifferent to the presence of outliers, providing a more realistic measure of trends in a time series than the typical linear regression (Fan and Wang, n.d.; Pereira et al., 2017; A. P. P. Santos et al., 2016; A. P. P. dos Santos et al., 2016a; Silva and Dereczynski, 2014)

$$f(t) = Qt - B \qquad \text{(eq. 4)}$$

where Q is the linear coefficient of the trend line and B is a constant. In order to estimate the slope Q, the first step is to calculate the slopes of all data pairs as follows:

$$Q_i = \frac{x_j - x_k}{j - k} \qquad \text{for } j > k \qquad \text{(eq. 5)}$$

Assuming n is the number of records in the time series, there will be $N = n(n\text{-}1)/2$ estimates *for Qi*. So, the method Sen assumes Q as the average of all values of Qi:

$$Q = Q_{[(N+1)/2]}, \quad \text{if } N \text{ be odd, and}$$

$$Q = \frac{1}{2}(Q_{[N/2]} + Q_{[(N+2)/2]}), \text{ if } N \text{ be pair.} \qquad \text{(eq. 6)}$$

Similar procedure is adopted to get the constant *B using the N* values for the difference $(x_i - Q_{ti})$.

The seasonal timeframes were defined as follows: the summer is from December to February (DJF); the fall season is from March to May (MAM); the winter is from June to August (JJA); and spring occurs from September to November (SON).

3. Results

3.1.   *Results from the data quality control procedure and Kriging interpolation*

The INMET provided the ground observations in 129 automated weather stations (AWS) operating in from 2005-2015 in the Brazilian Northeastern region (NEB). The number of AWS presenting reliable data was different from year to year as consequence of the operation and maintenance difficulties along the 10-years period. The kriging interpolation method requires at least 30 AWS providing surface solar radiation data for fitting the semivariogram function. Less than 30 AWS provided reliable data during the 2005-2007 period, and those years were not considered for the spatial interpolation. The Figure 4 shows all AWS providing solar radiation data in 2008-2015. So, the data acquired during this period were employed for the spatial interpolation and the following steps of this study.

3.2. Spatial interpolation

Figure 4 also presents a map for the annual average obtained from the kriging interpolation technique of daily total of global solar irradiation (Ig). The surface solar irradiance in the NEB is spatially heterogeneous either due to the regional topography or to the diverse meteorological systems reaching the region along the year.

The low cloud cover, especially in the backlands, explains the largest solar irradiance values. The maximum Ig occurs in an area encompassing part of the Bahia and Maranhão states where rainfall and the annual average of cloud cover are the lowest in the Brazilian territory. Figure 4 demonstrates that the coastal area in the North of the NEB, especially in the state of Rio Grande do Norte, receives the largest Ig values.
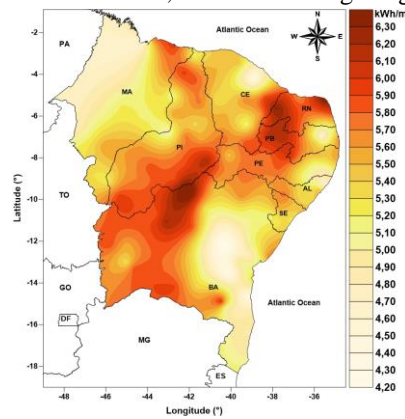
Figure 4. Map (kWh/m²) obtained by kriging interpolation of annual average of daily global solar irradiation data acquired at the 127 AWS operating in the Northeastern region of Brazil.

The lowest Ig values were observed in the Northwestern area of Maranhão, and in the Eastern coast area including Bahia, Sergipe and Alagoas states. This distribution pattern occurs as consequence of different meteorological phenomena like the Intertropical Convergence Zone (ITCZ), the frontal systems, the upper-tropospheric Cyclonic Vortices (UTCV), the easterly waves disturbances (EWD), the sea breezes and the trade winds.

The climate phenomena and their combination in different time and spatial scales may cause significant variations in the solar energy resource. Figure 5 presents the seasonal maps for global solar irradiation at the surface and the strong influence from the typical climate-specific mechanisms in each area can be identified in the spatial distribution patterns. The solar irradiation variability is intrinsically associated with the ITCZ movement during the year and change of the descending branch position of the Walker cell. Figure 5d demonstrates that the largest solar irradiation occurs during the dry season in the NEB (from September to November – Spring in the southern hemisphere). The season MAM (Figure 5b) depicts for the period with the lowest surface solar irradiation associated with the highest convective activity in the region linked to the ITCZ displacement to the north hemisphere (Nobre and Shukla, 1996).
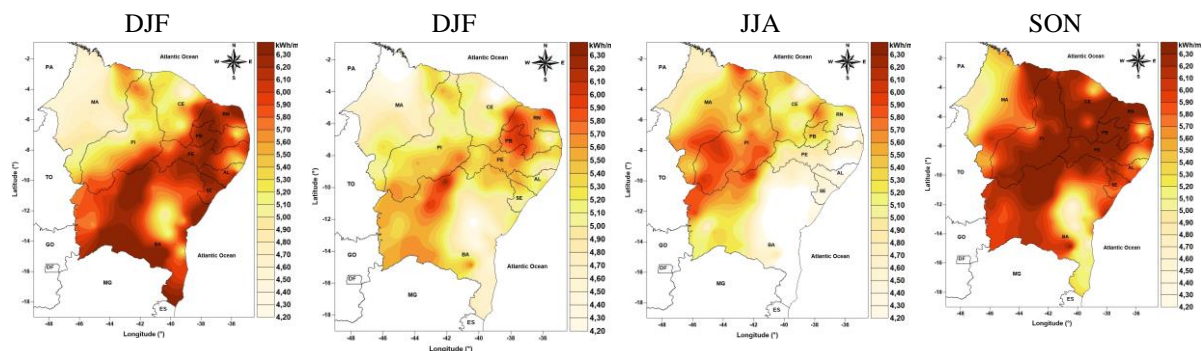
Figure 5. Seasonal maps for daily total of global solar irradiation (kWh/m²): (a) DJF (summer), (b) MAM (fall), (c) JJA (winter) and (d) SON (spring).

The low incidence of solar irradiation in the eastern area of the NEB during the seasons MAM and JJA can be described by the influence of the easterly waves disturbances and the frontal systems reaching the Equatorial latitudes, especially during winter (JJA) in the southern hemisphere. As mentioned earlier, the season MAM is the rainy season in the eastern coastal area and the solar irradiation achieves seasonal averages ranging between

4.30 and 5.80 kWh/m². The solar irradiation averages from 4.90 till 6.30 kWh/m² in the seasons JJA and SON. Such large solar irradiation values happen generally in the driest period of the year in the eastern coastal area of the NEB as indicated in Figures 6c and 6d. At this time of the year, the cloudiness associated with the ITCZ is located further north over the Atlantic Ocean (Molion and Bernardo, 2002). The lowest solar irradiation in the Southern area of the NEB, occurs during JJA and SON periods due to the influence of the frontal systems interacting with the local convection and precipitation.

3.3. Cluster Analysis (CA)

The CA analysis was performed using the geographical coordinates and the monthly average of the daily total solar irradiation as input data. The number of homogeneous regions was established taking into consideration the dendrogram presented in Figure 6. The dendrogram was obtained using the Ward method. The 127 stations are displayed on the horizontal axis, referenced by their ID's, and the vertical scale shows the similarity distance (or similarity level) between similar groups. The larger the similarity level, the more heterogeneous are the individuals inside a group of weather stations. The CA analysis provided five regions homogeneous using a subjective cutoff value for similarity level. The Figure 6 shows the homogeneous regions in different colors obtained using the Cutoff line in dendrogram. The cutoff threshold was chosen to provide homogeneous regions with a significant number of AWS in each one.
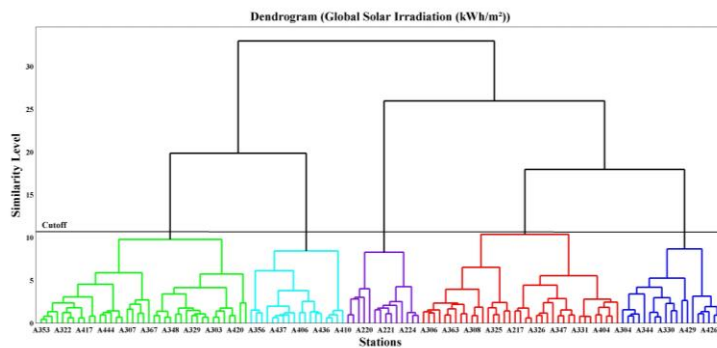
Figure 6. Dendrogram resulting from Ward method applied to the 127 AWS operating in NEB.
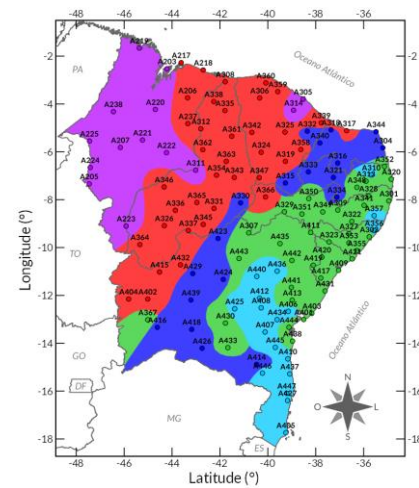
Figure 7. The five homogeneous areas (HR) regarding the surface solar irradiation in NEB. The colors are the same used in dendrogram shown in Figure 6: HR1, cyan; HR2, purple; HR3, green; HR4, Red; HR5, blue. The dots are the AWS's locations used in the cluster analysis.

The map in Figure 7 shows the geographical location of the homogeneous regions in NEB represented by the same colors used in Figure 6. There are some homogeneous regions divided into different areas of the NEB. Figure 7 also shows a strong spatial matching between the geographical location of the homogeneous regions and the spatial patterns observed in the interpolation map presented in Figure 4.

The geographical distribution of solar irradiation in NEB reflects the influence of the seasonal meteorological systems and environment features. The homogeneous regions 4 and 5 (HR4 and HR5) are the ones presenting the largest annual averages of surface solar irradiation. The lowest averages are observed in the regions HR1 and HR2 as indicated in Figure 8.

The HR4 and HR5 have a large territorial extension over the Northeastern backlands where climate dynamics and topography do not sustain the development of convective clouds. By contrast, the HR2 has a lower incidence of solar radiation due to the influence of heat and moisture from the Amazon region supporting a more convection activity than any other HR in NEB.

Figure 8 also provides information on the distinct seasonal cycles in each HR. Three of the HR areas (HR1, HR3, and HR5) present seasonal cycles in phase with the maximum (minimum) of the monthly average of the daily surface solar irradiation occurring in October/November (June). The other two regions, HR2 and HR4, also get

the highest monthly average values in September. However, both regions present very low variability along the first six months of the years (5 kWh/m^2) due to the intense convection systems in the Center-North of the NEB. The HR1 and HR2 have very close annual averages and a very low interannual variability, but the annual cycles are very different. The geographical distance among them is large and they have very distinct climatic characteristics. Similar behavior can explain the differences among HR3 e HR4. The HR5 receives the largest solar irradiance all year long.
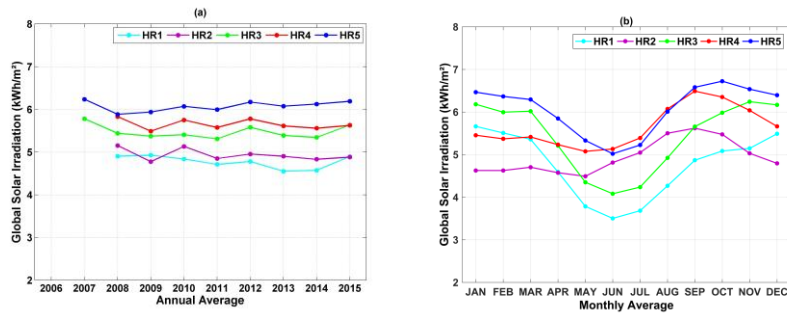
Figure 8. The annual and monthly averages of solar irradiation in the five homogeneous areas in NEB.

Figure 9 presents the boxplot analysis for incoming global solar irradiation in each homogeneous region of the NEB. The boxplot allows evaluating the inter-annual variability. The dot and line inside the rectangles represent the mean and the median values, respectively. The rectangles and vertical bars demonstrate the spreading of the annual average taking into consideration one-standard deviation and two-standard deviation interval, respectively. For the time-period under investigation, the HR2 and HR4 showed the lowest inter-annual variability. The HR3 has the largest variability with annual averages ranging between 3.7 and 6.7 kW/m², followed by the HR1 region (between 3.2 and 6.1 kWh/m²). The highest annual mean values occurred in HR4 and HR5, up to 7.1 and 6.8 kWh/m², respectively. The lowest annual mean global solar irradiation was in region HR1 (around 3.2 kWh/m²).

The inter-annual variability on a seasonal scale is presented in Figures 9b to 9e. The seasons MAM (fall) and JJA (austral winter) show the largest inter-annual amplitudes for seasonal averages in every homogeneous region. The seasonal averages for HR4 and HR5 are larger in season SON (spring). For other three regions, the seasonal averages are larger in summer (season DJF). This behavior is quite consistent with regional climatology for the spring season – low nebulosity in most of the Northeastern region.
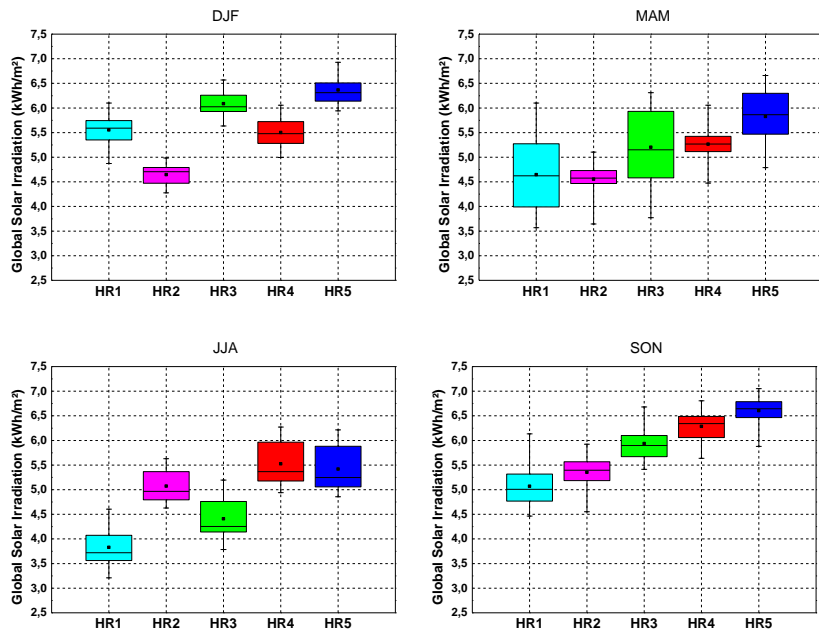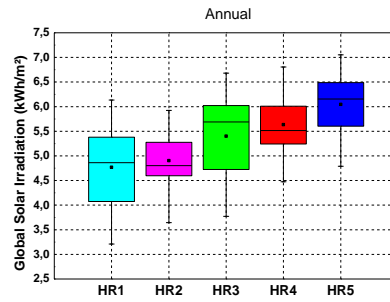
Figure 9. The inter-annual variability on seasonal scale are presented in (a) DJF (austral summer), (b) MAM (fall), (c) JJA (austral winter) and (d) SON (spring).

Figure 10 presents the trend analysis for the annual and seasonal averages of the surface solar radiation using the Mann-Kendall and Sen methods. The daily surface solar irradiation in HR5 showed an increasing trend with a magnitude of +0.04 kWh/m²/year and statistical significance of 90%. On the contrary, the surface solar irradiation in HR1 showed a decreasing trend around -0.05 kWh/m²/year with the statistical significance of 90%.

In seasonal scale, the surface global solar irradiation in HR1 presented a decreasing trend (around -0.05 kWh/m²/year) with the statistical significance of 95% during the seasons MAM and JJA. In RH5, the surface solar irradiation presented a trend around +0.04 kWh/m²/year in the season DJF and +0.07 kWh/m²/year in the season MMA. Other trends were identified but none of them presented statistical significance.
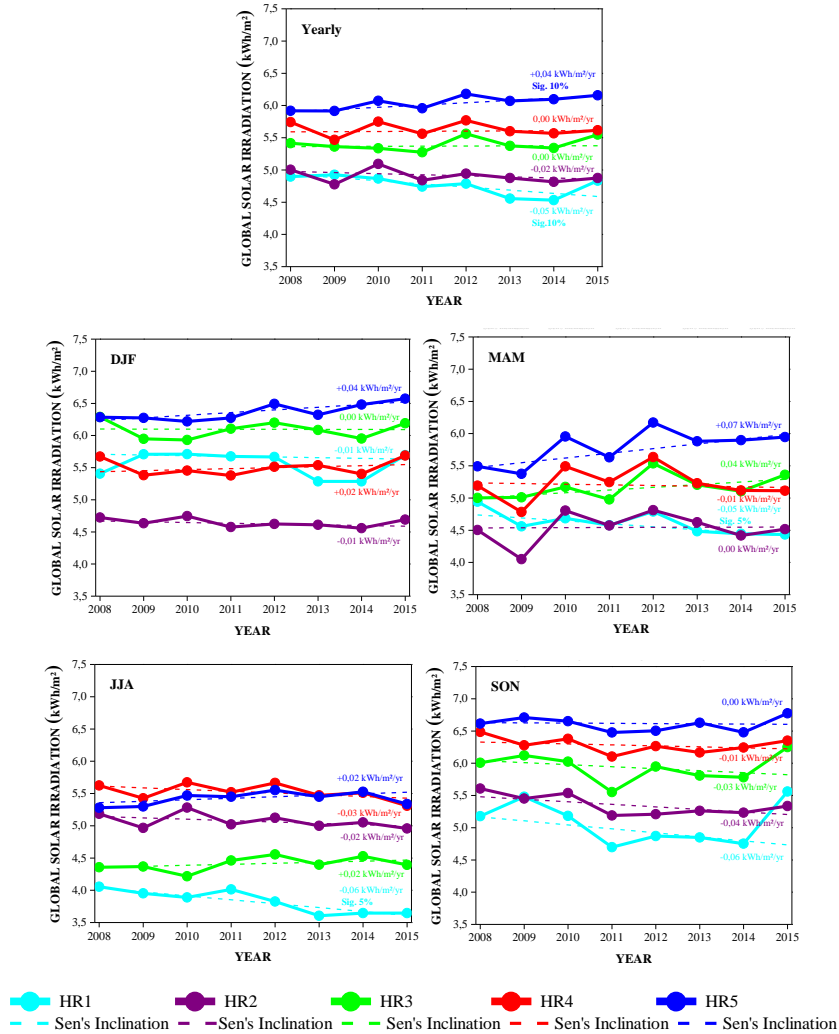
Figure 10. The temporal evolution of the annual and seasonal averages of daily total surface global solar irradiation (kWh/m²): (a) annual, (b) DJF season (summer), (c) MAM season (fall), (d) JJA (winter) and (e) SON season (spring). The graphs also shows the slope and magnitude of the trend obtained by using the Sen method and the Mann-Kendall test.

4. Conclusions

This work aimed at characterizing the surface global solar irradiation in the Northeastern region of Brazil based on statistical analysis of ground data acquired during the 2008-2015 timeframe. The cluster analysis pointed out five regions (HR) presenting distinct patterns regarding the incoming global solar irradiation in NEB territory. These five patterns (HRs) have a geographical distribution quite consistent with the climate features and typical meteorological systems operating in the NEB. The HR5 is the driest area, and it has the largest daily average of global solar irradiation. The southeastern area of NEB (HR1) has the lowest daily solar irradiation. The inter-annual variability is larger in the eastern and central area (HR3) of NEB due to the influence of several mechanisms to generate cloudiness. On the other hand, the smallest interannual variability occurs in the western area of NEB (HR2). The HR2 is the area presenting the largest nebulosity in NEB due to the influence of heat and moisture from the Amazonia region.

The austral summer season, from December to February, presents the smallest inter-annual variability of daily global solar irradiation, but not the largest averages in all homogenous regions. It is worthy to mention two opposite situations. First, the largest seasonal average of daily solar incidence in HR1 and HR3 occurs in the season DJF (summer). On the other hand, the smallest lowest seasonal average of daily solar irradiation in HR2 occurs in the same season (DJF).

The trend analysis demonstrates that the daily surface solar irradiation in the southeastern of NEB is decreasing by 50 Wh/m^2/year since 2008. On the other hand, the daily surface solar irradiation in HR5 (the semi-arid area) is increasing around 40 Wh/m^2/year along the same timeframe. It is worth noting that increasing frequency of climate events, such as ENOS, can influence these results.

Although there is a large solar energy resource in NEB, there are some particular issues related to the geographical distribution and the influence of typical regional climate features, which needs to be better known to support solar energy deployment. The results can help to understand the seasonal and inter-annual variability of the surface solar irradiation in NEB to meet the information demand from the energy sector. Besides that, these results are important to help in methodology development for short-term forecasts of solar irradiation taking into account the regional features and typical variability of the solar resource in NEB

5. References

Cavalcanti, I.F.A., Ferreira, N.J., Dias, M.A.F. da S., Justi, M.G.A., 2009. Tempo e Clima no Brasil, 1st ed. São Paulo.

Cohen, S., Ianetz, A., Stanhill, G., 2002. Evaporative climate changes at Bet Dagan, Israel, 1964-1998. Agric. For. Meteorol. https://doi.org/10.1016/S0168-1923(02)00016-3

Corrar, L., Paulo, E., Dias, J., 2007. Análise multivariada: para os cursos de administração, ciências contábeis e economia, São Paulo: Atlas.

Dobesch, H.., Dumolard, P.., Dyras, I.., 2010. Spatial Interpolation for Climate Data: The Use of GIS in Climatology and Meteorology, Spatial Interpolation for Climate Data: The Use of GIS in Climatology and Meteorology. https://doi.org/10.1002/9780470612262

Dobesch, H.., Dumolard, P.., Dyras, I.., 2007. Spatial Interpolation for Climate Data, Spatial Interpolation for Climate Data: The Use of GIS in Climatology and Meteorology. ISTE, London, UK. https://doi.org/10.1002/9780470612262

dos Santos, A.P.P., Coelho, C.A.S., Pinto Júnior, O., dos Santos, S.R.Q., de Lima, F.J.L., de Souza, E.B., 2018. Climatic diagnostics associated with anomalous lightning incidence during the summer 2012/2013 in Southeast Brazil. Int. J. Climatol. 38, 996–1009. https://doi.org/10.1002/joc.5227

Echer, M.P.D.S., Martins, F.R., Pereira, E.B., 2006. A importância dos dados de cobertura de nuvens e de sua variabilidade: metodologias para aquisição de dados. Rev. Bras. Ensino Física. https://doi.org/10.1590/S1806-11172006000300011

Fan, X.-H., Wang, M.-B., n.d. Change trends of air temperature and precipitation over Shanxi Province, China. https://doi.org/10.1007/s00704-010-0319-2

Goldemberg, J., Lucon, O., 2008. Energia, meio ambiente e desenvolvimento. Editora da Universidade de São Paulo.

Goossens, C., Beerger, A., 1986. Annual and Seasonal Climatic Variations over the Northern Hemisphere and Europe during the Last Century. Ann. Geophys.

Gu, L., 2003. Response of a Deciduous Forest to the Mount Pinatubo Eruption: Enhanced Photosynthesis. Science (80-.). https://doi.org/10.1126/science.1078366

Hair Jr., J.F., Anderson, R.E., Tatham, R.L., Black, W.C., 2005. Análise Fatorial. Análise Multivariada de Dados.

Journée, M., Bertrand, C., 2010. Improving the spatio-temporal distribution of surface solar radiation data by merging ground and satellite measurements. Remote Sens. Environ. 114, 2692–2704. https://doi.org/10.1016/j.rse.2010.06.010

Kayano, M.T., Andreoli, R. V., 2009. Clima da região Nordeste do Brasil, in: Off (Ed.), Tempo e Clima No Brasil. Oficina de Texto, São Paulo, p. 464.

Kousky, V.E., 1979. Frontal Influences on Northeast Brazil. Mon. Weather Rev. https://doi.org/10.1175/1520-0493(1979)107<1140:FIONB>2.0.CO;2

Lima, E. de A., Molion, L.C.B., Gomes Filho, M.F., Firmino, J.L. da N., Silva, A.O. da, 2007. Variabilidade interanual da profundidade óptica da atmosfera sobre Maceió, AL. Rev. Bras. Eng. Agrícola e Ambient. 11, 509–514. https://doi.org/10.1590/S1415-43662007000500010

Lima, F.J. de L., Castro Amanajás, J., Valter De Souza Guedes, R., Mariano, E., Silva, D., 2010. Análises de Componente Principal e de Agrupamento para estudo de ventos para a geração de energia eólica na região do Ceará, Paraíba, Pernambuco e Rio Grande do Norte, Brasil. Rev. Ambient. Água -An Interdiscip. J. Appl. Sci. 5. https://doi.org/10.4136/1980-993X

Lima, F.J.L., Martins, F.R., Pereira, E.B., Lorenz, E., Heinemann, D., 2016. Forecast for surface solar irradiance at the Brazilian Northeastern region using NWP model and artificial neural networks. Renew. Energy 87, 807–818. https://doi.org/10.1016/j.renene.2015.11.005

Lohmann, G.M., Monahan, A.H., Heinemann, D., 2016. Local short-term variability in solar irradiance. Atmos. Chem. Phys. 16, 6365–6379. https://doi.org/10.5194/acp-16-6365-2016

Martins, F.R., Pereira, E.B., 2011. Enhancing information for solar and wind energy technology deployment in Brazil. Energy Policy 39, 4378–4390. https://doi.org/10.1016/j.enpol.2011.04.058

Martins, F.R., Pereira, E.B., 2006. Parameterization of aerosols from burning biomass in the Brazil-SR radiative transfer model. Sol. Energy. https://doi.org/10.1016/j.solener.2005.03.008

Martins, F.R., Pereira, E.B., Abreu, S.L., 2007. Satellite-derived solar resource maps for Brazil under SWERA project. Sol. Energy. https://doi.org/10.1016/j.solener.2006.07.009

Martins, F.R., Pereira, E.B., Silva, S. a. B., Abreu, S.L., Colle, S., 2008. Solar energy scenarios in Brazil, Part one: Resource assessment. Energy Policy. https://doi.org/10.1016/j.enpol.2008.02.014

Martins, F.R., Rüther, R., Pereira, E.B., Abreu, S.L., 2008. Solar energy scenarios in Brazil. Part two: Photovoltaics applications. Energy Policy 36, 2855–2867. https://doi.org/10.1016/j.enpol.2008.04.001

Mello, C.R., Lima, J.M., Silva, A.M., Mello, J.M., Oliveira, M.S., 2003. Kriging and inverse-square-distance for the interpolation of rainfall equation parameters. Rev. Bras. Cienc. Do Solo.

Molion, L.C.B., Bernardo, S. de O., 2002. Uma Revisão da Dinâmica das Chuvas no Nordeste Brasileiro. Rev. Bras. Meteorol.

Mueller, T.G., Pusuluri, N.B., Mathias, K.K., Cornelius, P.L., Barnhisel, R.I., Shearer, S.A., 2004. Map Quality for Ordinary Kriging and Inverse Distance Weighted Interpolation. Soil Sci. Soc. Am. J. https://doi.org/10.2136/sssaj2004.2042

Nobre, P., Shukla, J., 1996. Variations of sea surface temperature, wind stress, and rainfall over the tropical

Atlantic and South America. J. Clim. https://doi.org/10.1175/1520-0442(1996)009<2464:VOSSTW>2.0.CO;2

Paixao, E., Auld, H., Mirza, M.M.Q., Klaassen, J., Shephard, M.W., 2011. Regionalization of heavy rainfall to improve climatic design values for infrastructure: case study in Southern Ontario, Canada. Hydrol. Sci. J. 56, 1067–1089. https://doi.org/10.1080/02626667.2011.608069

Pereira, E.B., Martins, F.R., Abreu, S.L. de, Rüther, R., 2006. Atlas Brasileiro de energia Solar, 1st ed. São José dos Campos.

Pereira, E.B., Martins, F.R., Gonçalves, A.R., Costa, R.S., Lima, F.J.L. de, Rüther, R., Abreu, S.L. de, Tiepolo, G.M., Pereira, S.V., Souza, J.G. de, 2017. Atlas Brasileiro de Energia Solar, 2nd ed. São José dos Campos.

Roderick, M.L., Farquhar, G.D., Berry, S.L., Noble, I.R., 2001. On the direct effect of clouds and atmospheric particles on the productivity and structure of vegetation. Oecologia. https://doi.org/10.1007/s004420100760

Roesch, A., Wild, M., Ohmura, A., Dutton, E.G., Long, C.N., Zhang, T., 2011. Assessment of BSRN radiation records for the computation of monthly means. Atmos. Meas. Tech. https://doi.org/10.5194/amt-4-339-2011

Santos, A.P.P., Júnior, P., Souza, O., Santos, R., Paes, A.P., Santos[1], D., Júnior[2], O.P., Barreiros De Souza[3], E., Azambuja, R., Quadro, S.R., Santos, D., 2016. Revista Brasileira de Geografia Física Variabilidade espaço-temporal e identificação de Eventos Extremos de Descargas Atmosféricas no Estado de São Paulo durante o Verão. Rev. Bras. Geogr. Física V. 09 N 02, 346–352.

Santos, A.P.P. dos, Aragão, M.R. da S., Correia, M. de F., Santos, S.R.Q. dos, Silva, F.D. dos S., Araújo, H.A. de, Santos, A.P.P. dos, Aragão, M.R. da S., Correia, M. de F., Santos, S.R.Q. dos, Silva, F.D. dos S., Araújo, H.A. de, 2016a. Precipitação na Cidade de Salvador: Variabilidade Temporal e Classificação em Quantis. Rev. Bras. Meteorol. 31, 454–467. https://doi.org/10.1590/0102-778631231420150048

Santos, A.P.P. dos, Lima, F.J.L. de, Souza, E.B. de, Pinto Júnior, O., Santos, S.R.Q. dos, 2016b. Application of cluster analysis in the identification of homogeneous regions for the cloud-to-ground lightning incidence in the state of São Paulo, Southeastern Brazil. Rev. Bras. Geogr. Física 9. https://doi.org/10.5935/1984-2295.20160155

Sen, P.K., 1968. Estimates of the Regression Coefficient Based on Kendall's Tau. J. Am. Stat. Assoc. https://doi.org/10.1080/01621459.1968.10480934

Silva, B.B. Da, Lopes, G.M., Azevedo, P.V. De, 2005. Balanço de radiação em áreas irrigadas utilizando imagens LANDSAT 5 - TM. Rev. Bras. Meteorol. 20, 243–252.

Silva, V. de P.R. da, Silva, R.A. e, Cavalcanti, E.P., Braga, C.C., Azevedo, P.V. de, Singh, V.P., Pereira, E.R.R., 2010. Trends in solar radiation in NCEP/NCAR database and measurements in northeastern Brazil. Sol. Energy. https://doi.org/10.1016/j.solener.2010.07.011

Silva, R.A.E., De, V., Da Silva, P.R., Cavalcanti, E.P., Dos Santos, D.N., 2010. Study of the variability of solar radiation in northeast Brazil. Rev. Bras. Eng. Agrícola e Ambient. 14, 501–509.

Silva, W.L., Dereczynski, C.P., 2014. Caracterização Climatológica e Tendências observadas em extremos climáticos no Estado do Rio de Janeiro. Anu. do Inst. Geociencias. https://doi.org/10.11137/2014_2_123_138

Sneyers, R., 1990. On the statistical analysis of series of observations. Secretariat of the World Meteorological Organization.

Tennant, W.J., Hewitson, B.C., 2002. Intra-seasonal rainfall characteristics and their importance to the seasonal prediction problem. Int. J. Climatol. https://doi.org/10.1002/joc.778

Ward, J.H., 1963. Hierarchical Grouping to Oprimize an Objective Function. J. Am. Stat. Assoc.

Wild, M., 2009. Global dimming and brightening: A review. J. Geophys. Res. 114, D00D16. https://doi.org/10.1029/2008JD011470

Wilks, D.S., 2006. Statistical methods in the atmospheric sciences, Statistical Methods in the Atmospheric Sciences.2nd ed.